A unified mechanism to support innate and learned use of visual landmark guidance in insects

Roman Goulard[1,*], Cornelia Buehlmann[2], Jeremy E. Niven[2], Paul Graham[2], and Barbara Webb[1]

[1]School of Informatics, University of Edinburgh, Edinburgh, UK

[2]University of Sussex, School of Life Sciences, Brighton, UK

[*]Corresponding author: Roman Goulard, romangoulard@gmail.com

Abstract

Insects can navigate efficiently in both novel and familiar environments, and this requires flexiblity in how they are guided by sensory cues. A prominent landmark, for example, can ellicit strong innate behaviours (attraction or menotaxis) but can also be used through learning as a specific directional cue to sustain navigation memory. However, the mechanisms that allow both pathways to co-exist, interact or override each other are largely unknown. Here we propose a model for behavioural integration based on the neuroanatomy of the central complex (CX) and adapted to control landmark guided behaviours. We consider a reward signal provided either by an innate attraction to landmarks or a long-term visual memory that modulates the formation of a local vector memory in the CX. Using an operant strategy for a simulated agent exploring a simple arena world with a single cue, we show how the short-term memory generated can support both innate and learned steering behaviour. In addition, we show how this architecture is consistent with observed effects of unilateral mushroom bodies (MB) lesions in ants that cause a reversion to innate behaviour. We suggest the formation of a directional memory in the CX can be interpreted as transforming rewarding (positive or negative) sensory signals into a geometrical attractiveness (or repulsion) mapping of the environment. We discuss how this scheme might represent an ideal way to combine multisensory information gathered during the exploration of an environment and support optimized cue integration.

Keywords — Modeling, Insect navigation, Neural network, Central complex, Mushroom bodies, Innate/learned visual guidance

1 Introduction

An open question in biology is how brains, from insects to mammals, can use sensory cues differently and with flexibility according to specific contexts [1]. Insect navigation provides an ideal system in which to explore this problem, because they face the need to constantly update their memory to forage to new food sources and face new dangers/obstacles on their way [2]. In this context, the substantial use made by central-place foraging insects of specific visual landmarks [3–9] means that efficient discrimination and

learning to direct their paths can be crucial.

To focus the problem, we consider the different effects that a single landmark cue can have on an ant's behaviour while learning to navigate to a food source. Naïve ants [7], like flies [10], express a strong innate attraction to a vertical bar, assimilated as a singular landmark; but when trained to find a feeder displaced from this landmark, the landmark can then be used as a reference to keep a constant relative heading and thus return to the feeder location [11]. This simple experimental paradigm already poses several key questions.

The first is how the insect brain controls the maintenance of a specific heading course [12]. Recently, the principle of encoding of orientation in insects has been uncovered following the discovery of a subset of cells (E-PGs) in the central complex (CX) functioning as an internal compass [13; 14] similar to mammalian head direction cells [15]. These cells have also been shown to be essential for insects to keep an arbitrary constant direction relative to a single cue [16], a behaviour known as menotaxis [12; 17], suggesting a central role in orientation behaviours in general [18; 19]. However, the neural architecture that allows the encoding of a desired heading and its comparison with an internal compass is still to be determined [16].

The second question is how innate and learned behaviour can interact [7], or more generally, how various parallel pathways controlling directed behaviour could be combined. Recently, Sun *et al.* [20] proposed a way to combine several navigation systems using a common architecture similar to the ring attractor formed by E-PG neurons. The simple summation of these orientation signals could be done directly and offered Bayesian optimal combination characteristics [21] that could support the robustness of insect behaviour [22].

However, a third issue arises from the fact that not all navigation systems will necessarily provide information in the form of a desired orientation. For example, models of memory encoding in the mushroom bodies (MB) generally assume the output takes the form of a goodness/badness value of an olfactory cue [23] or a familiarity value of visual scenery [24]. Therefore, the integration of these signals into an ongoing orientation behaviour requires an alternative explanation.

Here we propose an integrative and anatomically constrained model of the insect compass, following the model described by Pisokas et al. [25], combined with a steering mechanism inspired by the model previously proposed by Stone et al. [19], to drive both innate attraction and innate, and learned, menotaxis. With minor, biologically plausible adaptations, this can support the formation of a memory based on different sensory inputs. In addition, the scheme of the circuitry allows the integration of external inputs carrying only an information of goodness/badness to produce an appropriate steering. This architecture could therefore underlie the integration of both external and internal (proprioception) sensory inputs in the general orientation scheme of the insects' CX.

2 Methods and Results

2.1 Simulations

The model was implemented in python 3.6. Each neuron is represented by a simple firing rate model [26]. The activation rule is either a linear function of the input (linear simple perceptron) capped between 0 and 1/-1 (excitatory/inhibitory) or a logic function (active or inactive based on a threshold). The input function is the sum of the activity rate of the pre-synaptic neurons. The model simulations are conducted in a simple 3D environment containing a single black object (a vertical cylinder, a cube or a reversed cone; randomly assigned for each simulation) in a white background world. The 3D environment is a custom

implementation in python 3.6 using the pyopenGL library. The agent is placed at the beginning of the simulation in the center of a virtual arena of 100 length unit (*l.u.*) diameter and moves freely until it either reaches the border of the arena or exceeds 1000 time unit (steps). The agent has a constant speed of 0.25 *l.u./step*, thus the time limit corresponds 250 *l.u.* or 2.5 times the length of an optimal straight line to the edge of the arena. During each simulation a single object is placed randomly around the arena at 150 *l.u.* from its center. The innate exploratory behaviour is obtain by adding noise in the model steering behaviour ($\pm 10° s.d.$), therefore providing a basal exploratory behaviour independent from the CX model output.

2.2 Model overview

Brain structures/neurons and abbreviations	
CX	Central complex (brain structure)
EB	Ellipsoid Body (CX structure)
PB	Protocerebral Bridge (CX structure)
E-PG	CX neuron type
P-EG	CX neuron type
P-EN	CX neuron type
PFL3	CX neuron type
FBn	Fan-shape body (CX structure) neurons
MB	Mushroom bodies (brain bilateral structures)
vPN	visual Projection Neurons (inputs to the MB)
KC	Kenyon cell (MB multisensory neurons)
MBON	Mushroom body output neuron (output of the MB)
Vin	Visual innate attraction pathway

We start with a pre-existing model of the compass system in the insect brain [25]. This circuit in the CX (specifically in the EB) is composed of three neurons subset called E-PGs, P-EGs and P-ENs (section 2.4) constituting a so-called ring attractor [14]. We assume here a visual input to the E-PG neurons, and proprioceptive input to P-ENs, which causes an activity 'bump' that tracks the animal's heading. We extent this model to control steering by introducing two sets of PFL neurons (one controlling each turns, left and right) that have heterogeneous connection strengths from the E-PG (section 2.5); this sets a steering direction relative to the bump. We then suggest a mechanism by which these heterogeneous weights can be adapted during behaviour (section 2.6), effectively associating self-motion in a certain direction to a positive (or negative) reward (operant conditioning). This allows steering in a goal direction relative to the stimulus for any arbitrary offset of the bump relative to the stimulus. Finally, we consider how a MB output, signalling familiarity of a visual panorama, could be used as the reward input to the CX and hence establish steering in relation to a route or a visual homing memory (section 2.7). We show this model can account for ablation experiments in which the loss of one MB results in ants exhibiting innate instead of learned attraction (section 2.8).

2.3 Visual circuit

The first layer of the model is a simple visual processing stage. Vision is considered fully panoramic around the azimuthal dimension and from 0° to 80° in elevation (horizon line to the top, note the simulated world contains no information below the horizon). The visual system is segmented into 1296 visual units [$48x27$, inherited from the simulation resolution and the division of the azimuth (48 units) into 8 quadrants (6 units each)], homogeneously distributed on both dimensions. Each unit acts as an edge detector (figure 1B). For each unit, the summed intensity of the left (S_L) and right (S_R) half of its visual field is compared (the difference is divided by the sum for normalization) to obtain an index ranging from 0 (no edge) to 1 (vertical edge). The same process is used

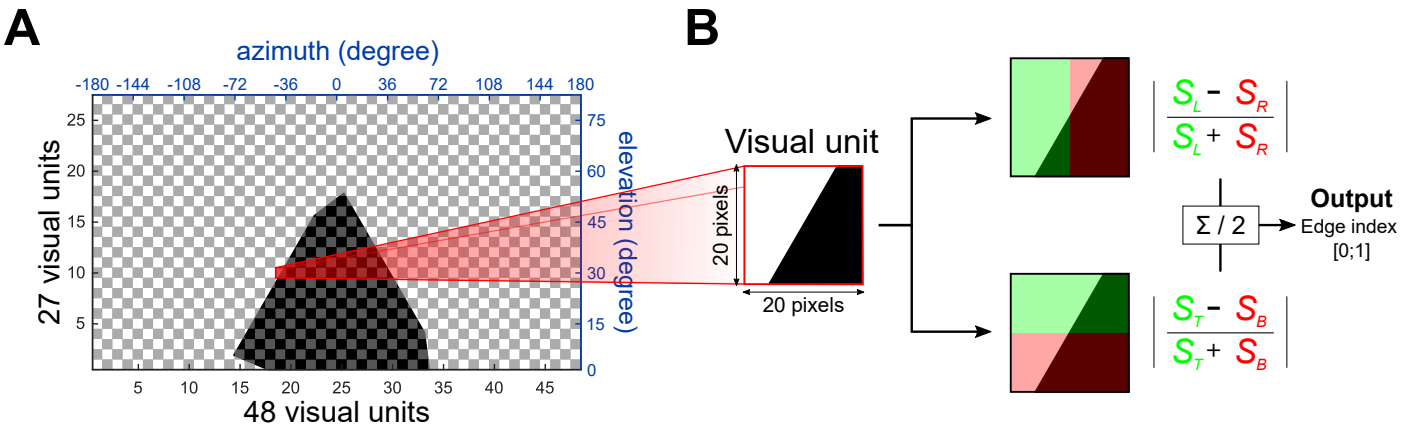

Figure 1: **Model visual system.**
A. Map of the 1296 (48x27) elementary units composing the visual system. The visual span is fully panoramic (360°) on the azimuth and 81° upward on the elevation. The red framed visual unit is the one used as example in **B**.
B. Elementary visual unit process. Each unit acts as a orientation-free edge detector. The comparison of the summed intensity of the left *vs* the right of the unit and of the top *vs* the bottom gives an index from 0 (no difference ↔ no edge) to 1 (corner edge) for each unit.

to compare the top (S_T) and bottom (S_B) half of the visual unit. Then, the two indexes for the vertical and horizontal edge are averaged to obtain the final output of the unit, a orientation-free edge index, ranging from 0 to 1:

$$\begin{aligned} Iv_i &= \frac{|S_{left} - S_{right}|}{S_{left} + S_{right}} \\ Ih_i &= \frac{|S_{top} - S_{bottom}|}{S_{top} + S_{bottom}} \\ I_i &= \frac{Iv_i + Ih_i}{2} \end{aligned} \tag{1}$$

Where Iv_i, Ih_i are respectively the vertical and hoizontal edge indexes, I_i the combined edge index, S_{left}, S_{right}, S_{top} and S_{bottom} are the 4 halves summed light intensity values.

2.4 Compass: Ellipsoid Body (EB) model

The main connectivity pattern in the EB model is taken from [25], which modeled the ring attractor function of the CX highlighted by neurophysiological studies in insects [13; 27; 28]. It is formed by four neuron types interacting together to create a ring attractor, three forming the excitatory part of the circuit, E-PGs, P-EGs and P-ENs, and one contributing inhibition, Delta7 [25]. The connective scheme between all these neuron types are organised in set of functional columns in two main parts of the CX, the EB and the Protocerebral Bridge (PB) but functionally form a ring [13; 25], as shown in figure 2A.

The visual input described above is segmented into 8 equal regions around the azimuth, which (in our model) connect in a retinotopic pattern with the first neuron type, the E-PGs (figure 2B). This retinotopic mapping has been made to simplify in the model the compass function derived directly from a single conspicuous bar, mimicking bar fixation experiment in *Drosophila* [13; 29]. Note that in fact, during bar following experiments, *Drosophila*'s EB bump expresses a constant, arbitrary offset with the bar's real position [13]. The real circuitry from vision to the EB in insects' brain is known to be more complex and involves the Ring neurons, which we will return to in the Discussion. We will also show that the steering mechanism we propose is not dependent on the retinotopic mapping but works for any arbitrary offset (section 2.6; figure S.4).

The inhibitory connections between E-PG neurons are considered global, as described in *Drosophila* brains [25]. The Delta7 inhibitory circuit is represented as a direct inhibition from each E-PG to all the other E-PGs. This creates a winner-take-all circuit, resulting in a single bump in neural activity that will follow the main contrast of the visual scenery. In the simulations here, this is usually a single object present in the otherwise homogeneous surroundings of the agent.

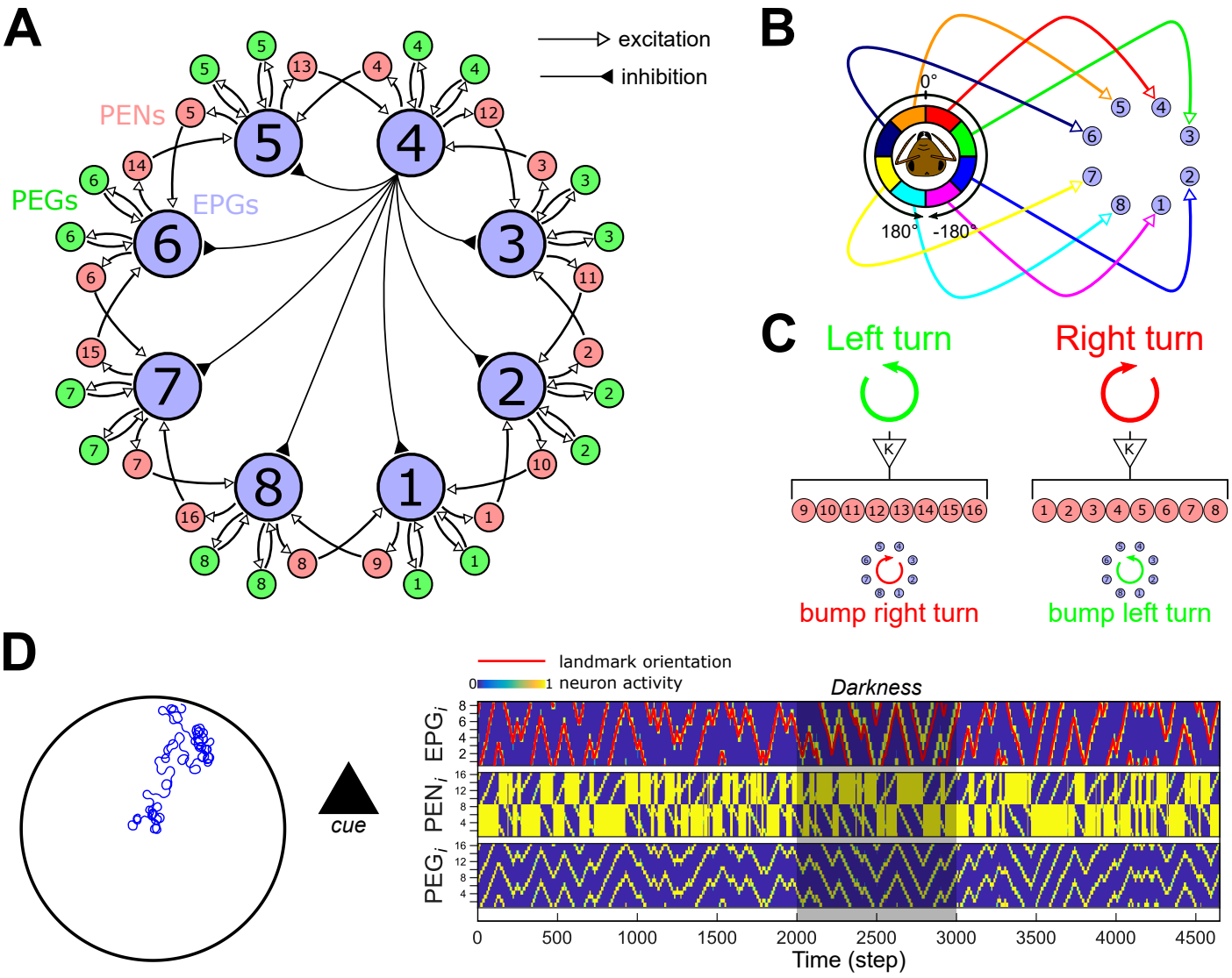

Figure 2: **Ellipsoid body compass model.**
A. Connectivity diagram between the main neurons of the EB-PB model, E-PGs, P-EGs and P-ENs. E-PGs have inhibitory connections with each other as indicated, via Delta7 neurons (black lines; one example is shown from the E-PG$_4$ in the central part of the diagram). E-PGs (light blue) form a recurrent circuit with P-EGs (green) while forming connection with neighbouring E-PGs through P-ENs (pink) on each side.
B. Connection diagram from the visual circuit to the E-PGs. Each angular segment connects in a retinotopic manner to the E-PGs. This will result in an activity bump forming in the circuit that corresponds to the direction of highest visual contrast.
C. Proprioceptive inputs to the P-ENs. When the ant agent is engaged in a left turn, P-EN$_{1-8}$ are stimulated, while during a right turn P-EN$_{9-16}$ are stimulated. This will trigger a counter-motion of the bump so that it still indicates the relative direction of the external cues.
D. Example of the function of the EB model in an arena surrounded by a single cue (here a cone represented by the black triangle). The left panel shows a random behaviour of the agent in the arena, intentionally including frequent rotation to highlight the cell activity and the compass function of the model. On the right panels are presented the activity of the different cell types. On the first line, the activity of E-PGs (blue for no activity to yellow for active) shows a perfect following of the cue orientation in the agent's visual field (red line). Even during a darkness episode (from 2000th to 3000th steps), the model keeps track of the cue position with a relatively low error thanks to the P-ENs role.

Inside the same column, E-PGs and P-EGs form a recurrent circuit, which allows the bump to persist in the absence of visual input. E-PGs also give presynaptic excitation to P-ENs from the same column, but P-ENs form presynaptic connections with E-PGs from a neighbouring column. In addition, we assume the P-ENs receive input from the proprioceptive sensory system (self-motion) through the Nodulus. The rotational speed of the agent is measured and injected as a binary input, 0 or 1 modulated by a fixed gain, to all the P-ENs on one side of the PB (P-EN$_{1-8}$ for a right turn or P-EN$_{9-16}$ for a left one, figure 2C). This causes the bump to be moved rightwards or leftwards around the ring, maintaining coherence of the bump position to the external cues even in darkness, as observed in the *Drosophila* brain [13]. The activity rate of each neuron group of the compass model is

set by the following set of equations:

$$\begin{cases} EPG_i(t) &= VU_i(t) + PEG_i(t-1) + PEN_{i-1|i+9}(t-1) - \sum \omega_{\Delta 7} EPG_j(t-1) \\ PEG_{i|i+8}(t) &= EPG_i(t-1) \\ PEN_{i|i+8}(t) &= EPG_i(t-1) \end{cases} \tag{2}$$

With VU_i the input from a octant of visual units (each octant connecting to a single EPG, see figure 2B) and $\omega_{\Delta 7}$ ($= 0.2$) the weight modulating the influence of each of the other EPG_j (with $j = 1, ..., 8$ excluding i) to the inhibitory pathway.

2.5 Steering: E-PGs to PFL3s heterogeneous connection scheme

A neurophysiological bridge from the compass to the control of motor behaviour has recently been identified in *Drosophila* [30]. This consists of a subset of neurons, the PFL3s (later also referred here simply as PFLs), that are downstream to the E-PGs, and upstream to the DNa2 neurons, bilateral descending neurons responsible for motor control and steering maneuvers [30]. Moreover, the PFLs are reported to represent the second largest input to these a2 neurons [31], supporting their important role. We therefore modelled the PFL layer to transform the compass bump into the motor command. We used *Drosophila* databases [31–34] to elaborate the connection scheme from EPG to PFL3 (figure S.2), forming synapses at the PB level. Each brain hemisphere possess 12 PFLs, which present synapses mainly with a single E-PG wedge. In the model, we simplified the conectome in the model to 16 PFLs (divided in to lateralized subset of 8 neurons) that connect the E-PGs upstream in a one-to-one scheme (figure 3A). In fact, a strict connectomic approach of the E-PG to PFL3 synapses (figure S.2) network shows that the PFL3 synaptics connections from the E-PG does not follow this homogeneity as some PFL3s share inputs from the same E-PG and no PFL3 neuron is reported to connect the 8th tiles of the PB. However, we made the choice to represent a one-to-one connection and rather evaluate the heterogeneity in the connectivity as a change in EPG-PFL synapses weights; but these could also be interpreted as the number of connections. The synapses between E-PGs and PFLs are represented as inhibitory as E-PGs are reported to be cholinergic synapses (figure 3A). The unilateral sum of the PFLs output is therefore considered to represent the motor signal received by each a2 neuron and their comparison gives directly the steering command.

To generate a steering signal in the PFL layer, we propose here that an heterogeneity in the distribution of the EPG-PFL synapses weights would be particularly adapted to give rise to a Left-Right inequality and thus a turn. More specifically, setting these weights in a particular pattern that frames the EB bump to the front of the visual field would suffice to generate an innate attraction to the conspicuous landmark (figure 3B). The detection of the cue in the right part of the visual field (as shown in figure 3A) would lead to an unbalanced inhibition of the PFLs and thus a diminished signal to turn left, thereby causing a right rotation and ultimately centering the cue in the frontal part (as cue detection in the left part of the visual field would have the opposite effect). When tested in the virtual environment, mimicking indoor arena experiments with a single landmark classically used in wood ants [11; 35], we observed accordingly an innate attraction behaviour toward the cue (figure 3C & D).

Assuming heterogeneous weights, allows the flexibility to shift the weight distribution to the right or the left (figure 4) to maintain the bump in a different position than the front of the agent. The subsequent oriented behaviour is opposite in direction to the switch of the EPG-PFL synapse weights, because they define the position in which the bump will be maintained during behaviour. Thus, by setting the weight accordingly, the model is capable of producing either direct attraction to a cue or menotaxis at any offset from the cue direction. We now go on to explore how the weights, instead of being arbitrarily defined as we have done in this section, could instead be learned through the agent's own experience to produce appropriately oriented behaviour in different contexts.

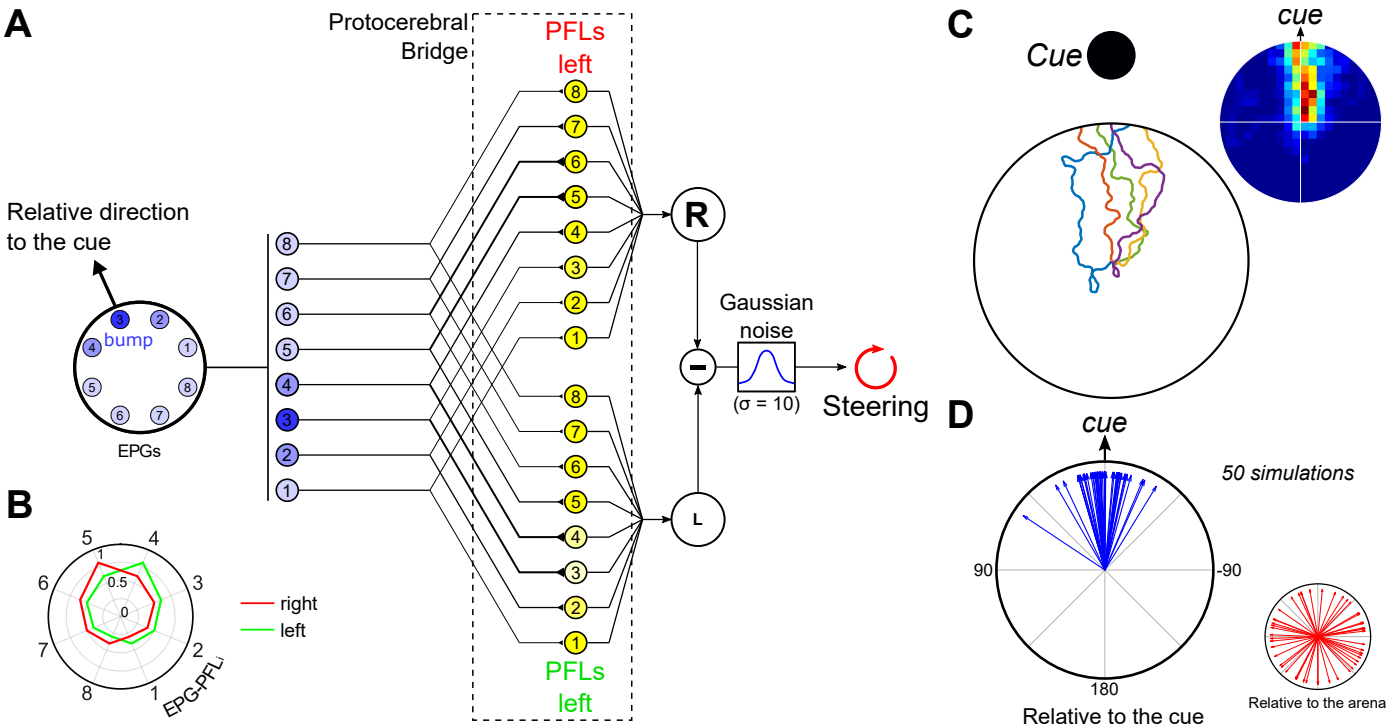

Figure 3: **EPG to PFL connectivity scheme.**
A. Diagram of the E-PGs to PFLs connectivity that drives the steering. Each E-PG makes inhibitory connection to two PFL neurons, one on each side. The strength of the synapse depends on the index of the E-PG$_i$ as shown in B. The summed activity rates of the right and left PFL neurons are compared to obtained the CX steering signal. Finally, gaussian noise ($\nu = 0$; $\sigma = 10$) is added to obtain the final steering command.
B. Synapse strength as a function of the index of E-PG$_i$. Synapses are inhibitory and therefore multiplied by -1. Red lines represent the connection with the subset of PFLs from the right part of the PB and green from the left part. Synapse weights are presented in a circular representation to show the correspondence with the E-PG input geometry. Index 1 corresponds to the synapse between ellipsoid body tile E-PG$_1$, connected to the rear right FOV (-157.5°), and PFL$_1$, and so on to index 8, the synapse between EPG$_8$, connected to the rear left (157.5°), and PFL$_8$.
C. Example of 5 simulation paths (randomly selected) toward a landmark. Top-right inset shows the heatmap in the arena for 50 simulations in total, the landmark direction being at the north.
D. Final direction/position of each simulation (n=50) with the cue placed in different positions around the arena, expressed in the cue (blue arrows) and the arena (red arrows, bottom-right inset) reference frames.

2.6 A memory to modulate the EPG-PFL connection weights

In order to allow ants to deal with different goals at different times, the mechanism that orients them with respect to landmarks, visual memories or other external information should allow some kind of plasticity or adjustment over time. Here we propose a mechanism that adopts some characteristics of the model proposed by [19] for path integration. Specifically, we add a set of units (similar to the CPU4 units in the [19] model) that get both compass and self-motion input, and implement a one column left or right shift before connecting to the steering neurons (PFL in our model - CPU1a in [19] model). However, in our case the motion input corresponds to left and right rotations rather than translation, and the output of these units is used to update the weights between the EP-G and PFL neurons, rather than directly contributing to steering (figure 5). [19] propose that CPU4 neurons (PF-LC in *Drosophila*), arborizing between the FB and the PB, could encode the memory for the path integrator. In contrast, here we propose that the modulation that would drive the use of landmarks could be represented rather by a direct plasticity between E-PGs and PFLs. The FB has shown the ability to encode a desired direction over a short period of time [36], we therefore consider it as a target for potential modulatory neurons and refer to the neurons in our model as FB neurons (FBn$_i$). In addition, we set the formation of this memory under the control of a global reward signal representing the sensory pathway(s) influence of the desired heading [16]. The aim of the weight modulation is to enable the formation of the same spatial weight pattern as presented in the previous section. The choice of a synaptic memory, instead of a memory accumulated in a FB neuron subset [19; 37], is primarily motivated by the permanent modification that could define the innate preference for vertical bars [3; 7]. However, we note that

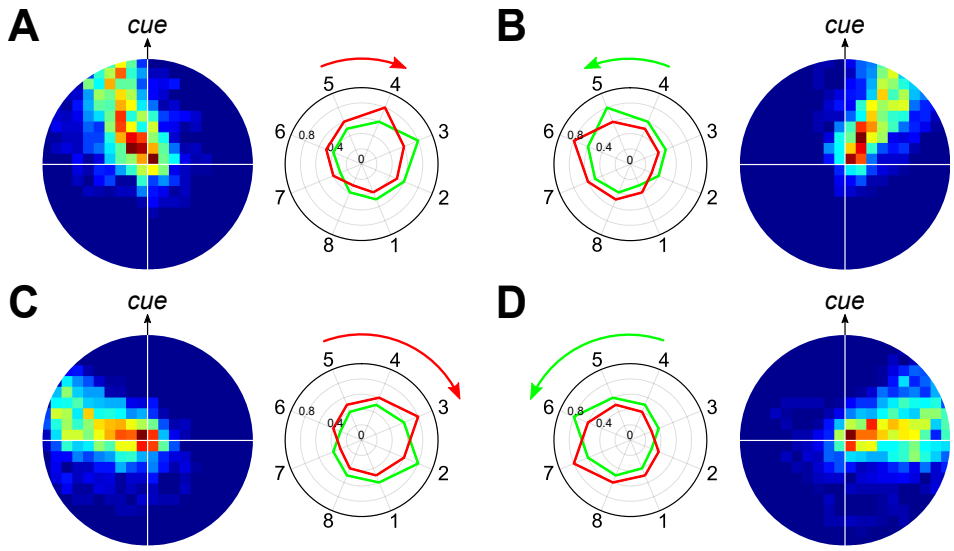

Figure 4: **Menotaxis induced by the shift of the heterogeneous EPG to PFL synapses weight.** **A.** Simulations (n=50 for each shift condition) where EPG-PFL synapse weights were shifted for 1 cell to the right/clockwise (compared to figure 3B). Results show the heatmap relative to the cue (top) of the 50 simulations. **B.** Simulations (n=50 for each shift condition) where EPG-PFL synapse weights were shifted for 1 cell to the left/anti-clockwise. Results show the heatmap relative to the cue (top) of the 50 simulations. **C-D.** Equivalent to A. and B. with a 2 cell shifs.

either solution would lead to the same mathematical formulation given the abstracted neural and synapse models used here. We rather focus on the potential of the functional columnar shift [19] and of the convergence of the three following components: the self-motion perception, the compass information and the influence of goodness-badness encoded sensory pathways. The FB neurons activity is set by the following equation:

$$\begin{cases} FBn_i^R(t) &= EPG_i(t) - NodR(t) \\ FBn_i^L(t) &= EPG_i(t) - NodL(t) \end{cases} \tag{3}$$

With Nod the inhibitory self-motion signal, from right ($NodR(t) = 1$) and left ($NodL(t) = 1$) turns respectively. Therefore $FBn^R(t) = 0$ during right turns and $FBn^L(t) = 0$ during left turns. Then, the EPG to PFL3 synapse weights are updated as follow:

$$\begin{cases} \omega R_i^{EPG-PFL}(t+1) &= \omega R_i^{EPG-PFL}(t) + \alpha\, FBn_{i-1}^R(t)\, Rew_{CX}(t) \\ \omega L_i^{EPG-PFL}(t+1) &= \omega L_i^{EPG-PFL}(t) + \alpha\, FBn_{i+1}^L(t)\, Rew_{CX}(t) \end{cases} \tag{4}$$

Where $\omega R/L_i^{EPG-PFL}$ is the synapse weight between E-PG$_i$ and PFL$_i$ on the right (R) or on the left (L) FB. The synapses are initialized in the model with a value of 0.5 and restricted between 0.2 and 0.8 during the simulations. α is a free parameter set equal to 0.001. The reward signal ($Rew(t)$) is set (as we describe below) to act as modulator for the synapse update by the FBns of the neighbouring functional column on the right (for the left PFLs) or the left (for the right PFLs).

The effect of equations 3 and 4 is as follows. Say the bump is centred on E-PG$_3$, as shown in figure 5, and the agent is turning right and observes a view which elicits a reward above threshold from any sensory system. The right FBns being inhibited by the right turn, the left FBns will induce an increase, under the control of the high reward level, in the EPG-PFL synapse shifted by one column to the left virtually (counter-clockwise) from the E-PG bump, on the E-PG$_4$. This leads to the increase of the tendency to turn right (EPG to PFL synapses being inhibitory) if the cue was to appear on the left of its current orientation. By exploring the environment, this mechanism creates therefore two weight distributions that frame the maximally attractive orientation.

To reproduce the innate attraction to a simple cue, widely observed in insects [38; 39], we create a reward signal directly from the visual processing. The aim is to have reinforcement of the signal from the foveal ommatidias (i.e. when facing the cue). This can be done using a mask on the visual units as shown in (figure 6, top panels). The mask is multiplied with the visual input and

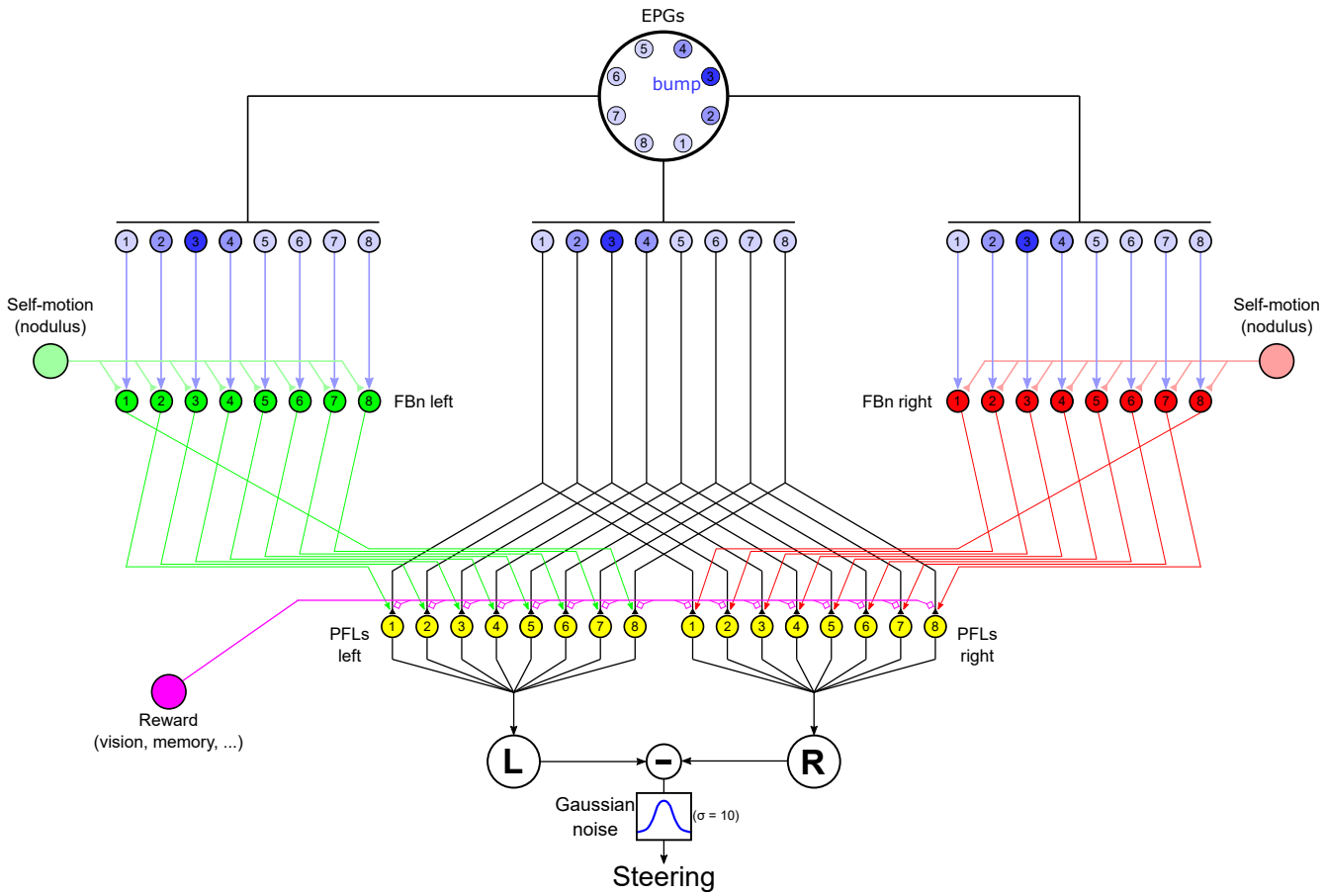

Figure 5: **Steering CX model with external control.**
The central part of the diagram is similar to the model of EPG to PFL connection presented in figure 3A except the synapse weights are initially set homogeneously ($\omega_i^{EPG-PFL} = 0.5$). On each side the model copies the [19] model architecture such that the connection between FBns [red (right FBns) and green (left FBns) cells] and steering neurons (PFLs, yellow cells) are shifted by one column, oppositely on each side. FBns also receive rotating self-motion inhibiting inputs [light red (right turns) and green (left turns) lines] for the ipsilateral side, therefore the right FBns are activated during left turns and viceversa. The reward signal (pink) is provided by the sensory pathway indicating goodness-badness of the environment. The steering command is obtain by comparing the right and left summed activity of the PFLs after the addition of a gaussian noise ($\nu = 0$; $\sigma = 10$) as previously (figure 3A).

the output summed across all units to provide the reward signal:

$$Rew_{CX}(t) \quad = \quad \sum M_i \; I_i(t) \tag{5}$$

With Rew_{CX} the CX reward signal used to update the EPG-PFL synapses, I the edge detection matrix (equation 1) estimated by the visual units (figure 1) and M the mask matrix (same size as I). We tested alternative masks (M) with either a sharp or graded preference for a frontal orientation of the strongest contrasts, and either with or without negative responses for contrasts at the rear of the visual field. In the case of the smooth masks, figure 1C & D) the reward signal is roughly proportional to the azimuth orientation of the strongest contrasts in the visual field. In the case of a single landmark environment, the use of such mask means the reward signal will reinforce the weights so as to center this landmark in the visual field.

Using the architecture presented in figure 5, we show its capability to generate a memory able to drive an innate attraction behaviour toward a single cue (figure 6). Note however that the reward condition with a proportional positive mask only (figure 6A) is not successful. Indeed, if the trajectories to the edge of the arena appear straight (comparison to exploratory behaviour without CX inputs shown in figure S.1) the general direction taken appears almost random, only showing a small trend to the half of the arena where the landmark is displayed. This is due to the positive reward that exists on the whole the panoramic visual field and therefore generates an oriented behaviour toward a random direction. This can be seen in the weight distributions generated in

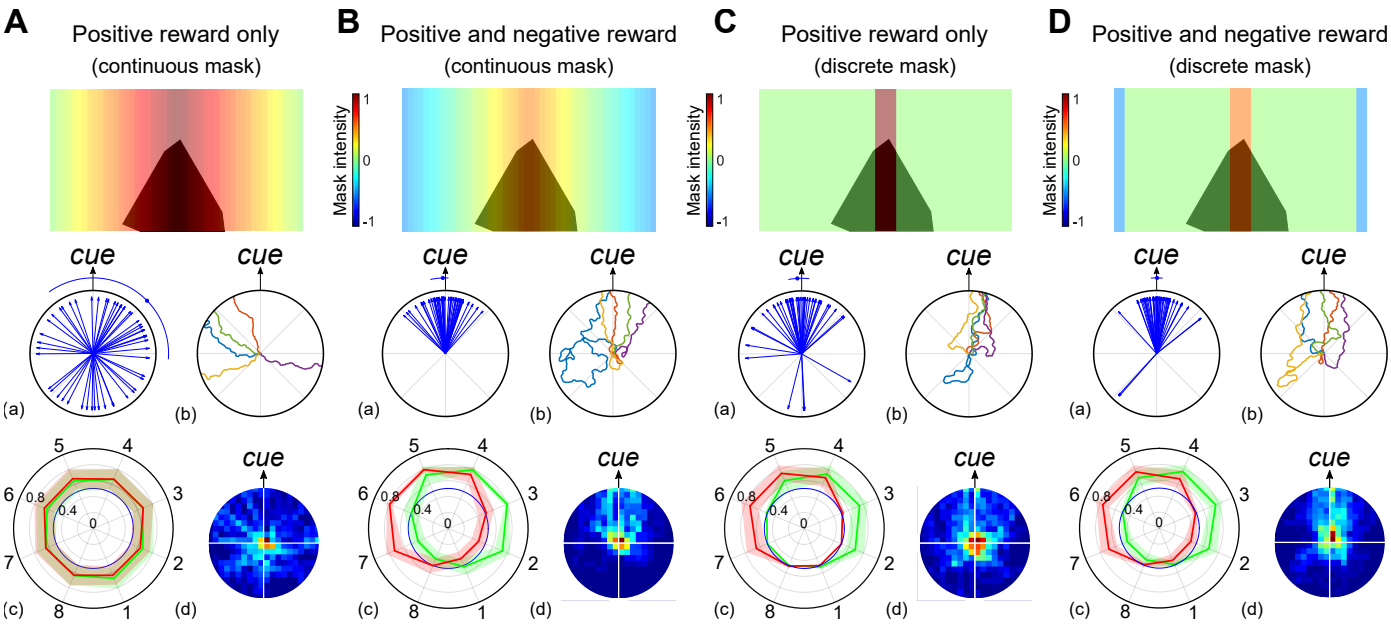

Figure 6: **Innate attraction under the control of a visual reward signal.**
Simulations of the FB steering model (figure 5) using a reward signal provided by the visual processes to modify the EPG-PFL synapse weights. We created the visual input signal to the CX using different masks. Results for each panel include (a) the final path directions (n = 50 simulations), (b) examples of 5 simulation paths, (c) the averaged EPG-PFLs synapse weights and (d) a heat map of the agent's location.
A. Visual input to the FBs is equal to the sum of the visual units signal through a continuous proportional mask from 0 (rear units) to 1 (frontal units).
B. Visual input to the FBs is equal to the sum of the visual units signal through a continuous proportional mask from -0.5 (rear units) to 0.5 (frontal units).
C. Visual input to the FBs is equal to the sum of the visual units signal through a discrete mask equal to 0 (outside the 30° frontal area) or 1 (inside the 30° frontal area).
D. Visual input to the FBs is equal to the sum of the visual units signal through a discrete mask equal to 0 (outside the 30° frontal area and the 30° rear area), 0.5 (inside the 30° rear area) or 1 (inside the 30° frontal area).

individual simulation, where the averaged weights did not show any orientation preference (figure 6A). However, the addition of a negative reward (when the cue appears on the rear of the visual field) clearly corrects this problem (figure 6B). This is of interest considering that insects are known to associate (innately or learned) positive or negative value to olfactory [40] and/or visual cues [2]. Even in the case of discrete filters, which did not carry any prior information of the cue's relative orientation, the model generates a consistent behaviour and coherent weight distribution for the E-PG to PFL3 synapses (figure 6C). Again, the use of both positive and negative sensory inputs to the model improves the performance (figure 6D). Furthermore, the modification of the mask, to reward the cue in a shifted position, produces an oppositely shifted behaviour (figure S.2), showing the ability to use the sensory information to drive oriented behaviour toward and/or away from a landmark, similar to menotaxis [12; 17].

Note that for these results, the bump and the landmark which generates the attraction were directly attached, i.e., the compass represents a truly allocentric compass based on the landmark. In contrast, in the insect brain during bar-following paradigms it is known that while the movement of the E-PG bump follows the bar movement, the actual position of the bump has an apparently random offset from the bar azimuth [13]. To explore this, we reproduced such an offset between the EB bump and the visual cue's position in the visual field by applying a random shift in the connectivity between the visual units and the E-PGs (figure S.4A). This means each simulation expresses a unique offset between the bump and the landmark. However, the innate attraction behaviour to the cue produced by the model is unchanged (figure S.4B). Statistically (across all runs) the EPG-PFL synapses weights generated by the simulation cannot show any oriented behaviour (figure S.4C), due to the random offset generated, but looking at the individual simulations we can see that the model defines the right set of weights to drive the behaviour toward the landmark in any situation (figure S.4D). Therefore we can conclude that the model does not use the bump as an absolute compass but rather

as a reference point to use another signal (here a valence signal) to define the orientation to take.

2.7 Using the Mushroom bodies familiarity memory

In addition to using a single visual input to generate an innate attraction to single object, as described above, we also tested how the output of the Mushroom Bodies (MB), a bilateral structure tightly associated with memory in the insects brain [41], could be used to generate a local memory in the CX to control appropriate orientated behaviour. To do so, we adapted the model of familiarity encoding for route memories that has been hypothesised to occur in the MB in social insects [24], and use the output as the reward input in our model. Recently, experimental results have supported the importance of MBs to view-based memory and navigation in ants [11; 42; 43].

The MB is modeled as a network (figure 7A) composed of 10000 Kenyon cells (KCs) sparsely connected each one with 3 to 5 visual Projection Neurons (vPNs). vPNs are directly taken as the outputs of the visual units calculating the edge indexes from the panoramic view (figure 1). The long-term memory is formed by a simple associative learning rule at the interface between the KCs and the output of the MB (MBON). The MBON signal is calculated as the sum of the KCs activity [KC_i - binary, either 0 (active) or 1 (inactive)] weighted by their associated synapse weight (ω_i^{vPN-KC}) and normalized by the number of KCs active, thus maintaining the MBON value between 0 and 1:

$$MBON = \frac{\sum \omega_i^{vPN-KC} KC_i}{\sum KC_i} \tag{6}$$

The vPN-KC synapses weights are initially set as 1 and updated under the control of a rewarding signal (DAN) with the following rules:

DAN(t)	KC$_i$(t)	$\Delta\omega_i^{vPN-KC}$(t+1)
0	0	0
0	1	0
1	0	0
1	1	-0.2

Where $\Delta\omega_i^{vPN-KC}$ is the change applied to ω_i^{vPN-KC}. The DAN activity is set to 1 during learning episodes and to 0 otherwise. To generate the visual memory during these learning episodes, the agent is placed at mid-distance between the center of the arena and a virtual feeder (always at 0° at the edge of the arena) and scans the environment during 100 time steps over a range from $-15°$ to 15° centred on the feeder (figure 7B). This range is chosen to match the span of the discrete visual mask (figure 6C). Following the update rules, which decreases the synapse strength from KC to MBON during learning episodes, the weaker the signal from the MBON, the stronger the familiarity of the current visual scene. Therefore, the MBON output is translated into a positive reward for greater familiarity, ($Rew_{CX}(t) = 1 - MBON(t)$), and used to influence the E-PG to PFL weight updates as before. To avoid the influence of the noise at low familiarity, we ignored any input signal from the MB to the CX lower than 0.5.

Using the MB familiarity level the model is able to direct the behaviour of the agent toward the feeder location (figure 7C & D). Despite the restriction of the memory to a single location, and the noisy familiarity observed during the simulations, the model is able to induce quite straight behaviour toward the goal location sometimes after expressing an initial erratic behaviour, due to the steering noise only. The averaged EPG-PFL synapses weights clearly show a pattern to keep the cue in the correct orientation [$\approx 45°$ on the left (counter-clockwise)] to reach the virtual feeder (figure 7E) Both innate attraction and MB memory can be actived to modulate the memory concomitantly (modulated by individual pathway gains, see section 2.8), resulting in a greater spread in the orientation toward the feeder goal (figure S.5A). However, the combination of both pathways highlights the importance of the self-motion integration in the model (figure S.5B-C).

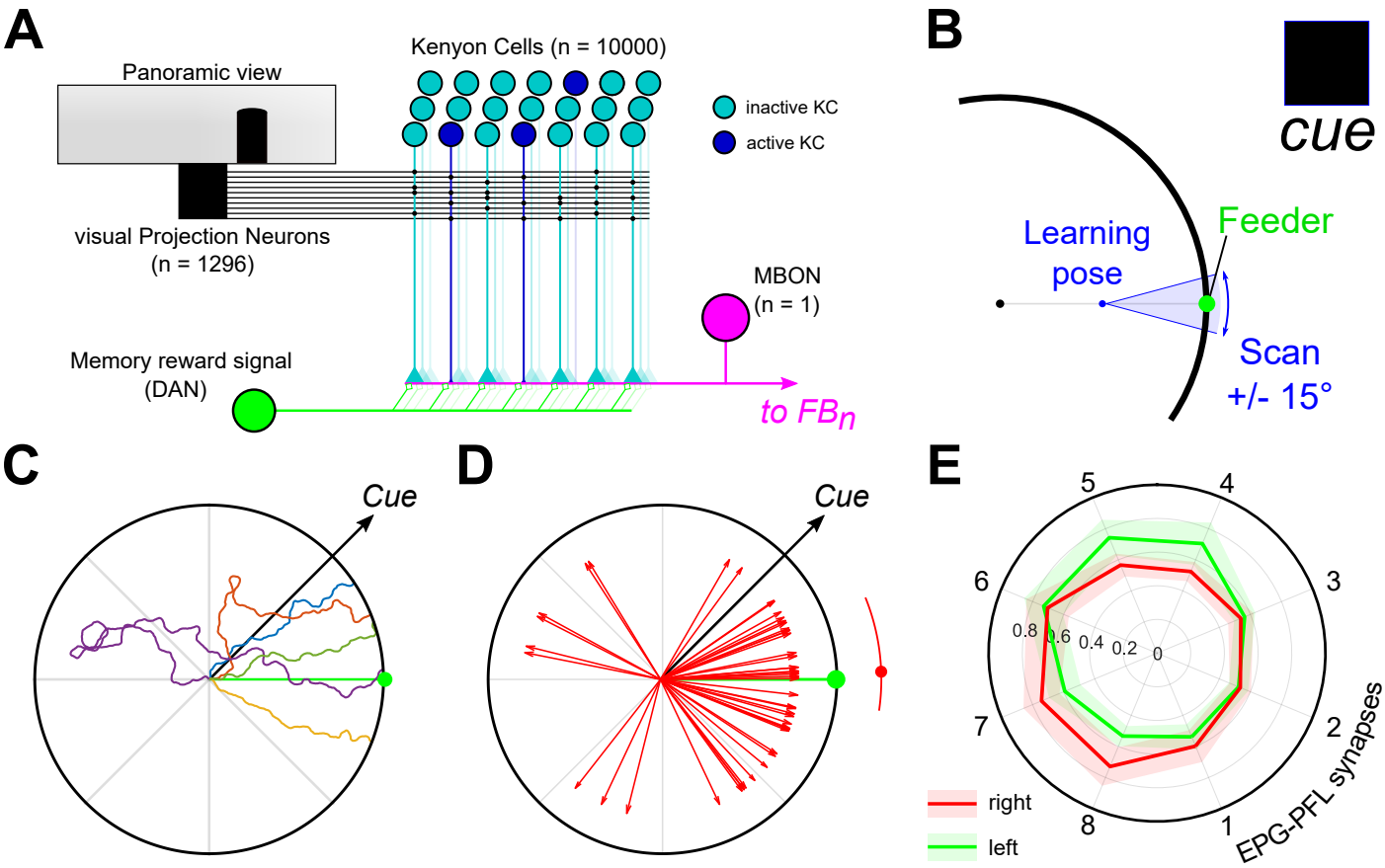

Figure 7: **Memory related behaviour.**
A. MB model diagram. The visual Projection Neurons (vPN) correspond to the visual units (figure 1) extracting edge from the panoramic view. Each KC present a random post-synaptic connection pattern with 2 to 5 vPNs and a pre-synaptic connection to the MB output neuron (MBON). During the learning procedure, the memory reward signal is activated and induce the decrease of the synapses between the activated KCs and the MBON. **B.** Learning phase diagram. The agent face the feeder during 100 steps from a position in between the feeder and the center of the arena (learning pose), with an orientation error from -15 to $15°$. MB model memory is updated during this phase (DAN active).
C. Paths example of retrieval experiment using the MB model as an input for the CX model.
D. Final direction vectors for 50 simulations with the feeder at $0°$ and the cue oriented at $45°$. The red arc shows the median (dot) 95% C.I. obtained by bootstraps (rep = 10000).
E. Averaged right (red) and left (green) EPG-PFL synapses weights (shaded area: $\pm s.d.$) obtained during 50 simulations.

2.8 Lesion experiments

In order to link our model to biological experiments [11], we set up simulations where the MB could be silenced completely. The first step was to duplicate the MB used in previous simulation to obtain two bilateral identical structures. Both MB follow the same vPN-KC connectivity parameters (similar as previously mentioned, figure 7A), but their connectivity is independent, and they are both connected homogeneously to the full panoramic view of the agent, i.e., the connectivity with both eyes is presupposed identical (figure 8A). The MBs output consist on each side of a single MBON neuron which input into the FB neurons of the same side only. Therefore the ablation of one MB deprives the ipsilateral FB neurons from any memory related inputs. To keep the model to the simplest case scenario we linearly added both innate visual (Vin) and MB inputs to generate a common reward signal to control the memory as follows:

$$Rew_{CX}(t) \quad = \quad \omega_{MB}\, MBON(t) + \omega_{Vin}\, Vin(t) \qquad with \begin{cases} \omega_{Vin} & \in \quad [0.0; 2] \\ \omega_{MB} & \in \quad [4.0; 10.0] \end{cases} \tag{7}$$

With Vin the signal provided by the visual mask (see equation 5), ω_{Vin} the gain modulating the visual innate attraction pathway and ω_{MB} the gain modulating the MB pathway. The range of the pair of gains as been choosen in a range that clearly advantages the MB pathway to obtain a behaviour oriented toward the surrounding of the feeder location (figure 8B), mimicking

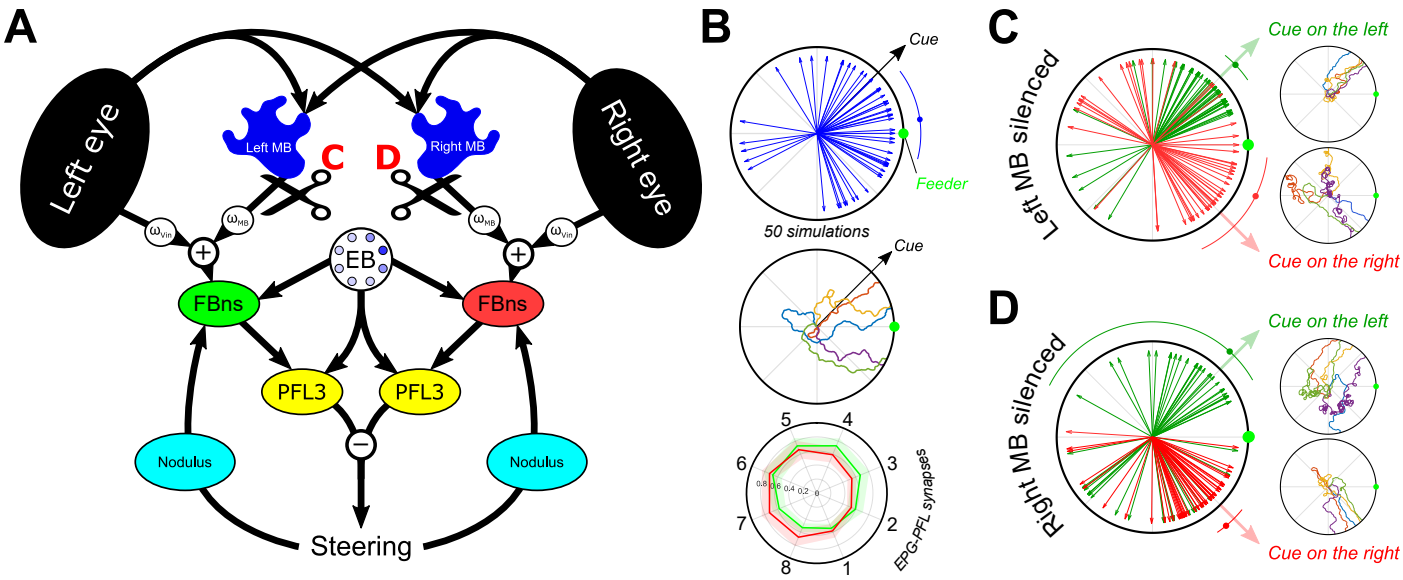

Figure 8: **Replication of unilateral mushroom body lesion experiments from [11].**
A. Schematic of the model including both MB and innate visual attraction. Both elements are linearly summed to form a single reward signal, using individual weights (ω_{Vin} & ω_{MB}) to modulate the influence of each component. Lesions are indicated by the black scissors and the results are reported in **C** and **D** (Left and right lesion respectively).
B. Simulation with the combination of innate attraction (ω_{Vin}) and the mushroom bodies (ω_{MB}) pathway. The learning procedure is similar as presented in figure 7B. From top to bottom, final directions (blue arrows, $n_{sim} = 50$) taken during the simulations [blue arc indicate the median (dot) 95% C.I. obtained by bootstrap ($n_{rep} = 10000$)], examples of path obtained during simulations, and averaged right (red) and left (green) EPG-PFL synapse weights (shaded area: $\pm s.d.$) obtained during 50 simulations.
C. Unilateral lesion of the left mushroom body. Final direction vectors and example paths.
D. Unilateral lesion of the right mushroom body. Final direction vectors and example paths.

the real behaviour of wood ants [11].

When an MB is unilaterally silenced and the agent presented with a landmark at $\pm 45°$ from the feeder, the model reverts to a strong attraction to the landmark in all cases (figure 8C-D). This is due to the importance of both EPG-PFL distribution (e.g., one on each side of the CX model) to define the orientation in which to keep the EB bump. With only one of the two, the MB memory does not influence the position of the bump and therefore only the innate attraction to the landmark actually influences the behaviour. Nevertheless, when the lesion is on the contralateral side of the position of the landmark from the feeder [i.e., Right (left) lesion with the cue on the left (right)], we observed an increase of looping behaviour (figure 8C-D, *examples panels*). Consequently this looping behaviour increases the noise observed in the final orientation taken by the model which could be consistent with a tendency observed in ants [11], suggesting the unilateral influence of each MB.

3 Discussion

Our principal objective was to build an neuro-anatomically inspired neural network model [19; 25; 30] able to explain the use of the EB compass as a reference to maintain a heading course toward a desired direction [16]. We first showed the potential of a specific weight distribution from the compass to PFL3 neurons to realise this task (figure 3 & 4). This is achieved thanks to the segmentation of these neurons into two unilateral subsets controlling independently turns on each side. This organisation corresponds to a more basic, probably ancestral, control scheme called tropotaxis [37] where the left-right comparison of a sensory signal drives the course to take [44]. We show here how this left-right structure of the CX output could be co-opted by sensory pathways (visual attraction and MB long-term memory) that do not themselves have such a left-right structure, through an adaptively acquired distribution of weights between the EB compass bump and the PFL3 neurons. The approach uses a known anatomical shift between functional columns that exists in the CX to build a memory of the relationship between self-motion and the compass signal, following a similar

principle to the path integrator described in [19]. Modulating a synaptic memory formation under the control of external sensory inputs that provide reward information, we showed how this architecture was able to drive oriented behaviour; mimicking both innate attraction to a bar [7; 10] and reaching a memorized location [11]. Such a memory process is coherent with the CX central role in spatial learning [45] as well as the storage of short-term orientation memory [46]. Moreover, we showed, in correspondence to experimental results observed in wood ants with unilateral MB lesions [11], that the model reverts to innate behaviour after similar simulated lesions, highlighting the importance of both MBs in memory view-based navigation.

3.1 Assumptions in the model about CX input

In this work, the main shortcut that abstracts from neuro-anatomical reality is the connection from the visual system to the EB, which in our model is a direct retinal input. Indeed, it is known that the visual inputs to the E-PGs, known as Ring neurons, are not retinotopic. Ring neurons connect from the Lateral Triangle (LTR) to the EB [29]. LTR glomeruli shown a conserved retinotopic organisation, with wide receptive fields which could increase the robustness of the visual encoding [47]. Post-synaptic connections of ring neurons in the EB include all the E-PGs, each with the potential to be modulated by neuronal plasticity [48]. The effect of this connection scheme is that an arbitrary offset can arise between the external location of a visual cue and the EB bump in bar following experiments [13]. Although we did not explicitly include ring neurons, we could simulate this offset by a retinotopic shift in the connection from vision to EB, and we showed how the model was able to work despite this offset (figure S.4). The representation of innate attraction as a modulatory signal and not as an intrinsic hardwired system allow this flexibility. Alternatively, the apparent randomness of some menotactic behaviour in insects could be explained by a hardwired architecture, where some arbitrary bump offset would fix the preferred direction. The difference of behaviour (direct attraction or menotaxis) observed in different species in different contexts [wood ants [7; 9; 11] and flying *Drosophila* [49] attracted by landmark *vs* walking *Drosophila* keeping a constant angle to a landmark [16]] argues for some flexibility in insect oriented behaviour.

The second input to modulate the memory in the model is the self-motion perception. The interaction of optic-flow and compass-mediated signals has already been proposed in the form of a speed measurement for the path integrator [19]. However, in our model, the crucial self-motion perception is of rotation. The ability of insect visual systems to untangle of the optic flow generated by translation and rotation [50] could support such a choice. Nevertheless, the implementation here is highly inferential; the existence of a pathway through the noduli to the EB is known [13] but the potential connections it could make to the FB is not. In our model, we found that the main advantage to select, specifically, an ipsilateral inhibition (i.e., right turns inhibit right FBns and left turns inhibit left FBns) was to facilitate the exploration and the integration of several cues (innate and memorized). A contralateral inhibition, for example, would lead to the attraction to the stronger cue and to the neglect of sparsely accessible cues such as the MB long-term memory (figure S.5).

Finally, a key component of the model is represented by the reward signal extracted from sensory pathways. The FB represents an ideal target to model the influence of parallel sensory pathways on the CX [37] because it receives inputs from several other brain areas, including the MB [51–53], while sharing the columnar organisation observed in the EB and the PB [14]. For example, *Drosophila* FB has been shown necessary to the control of the steering in a visual pattern recognition paradigm [54], involving the EB [55]. In addition, the CX is one of the main structures in the insect's brain, along with the MB, receiving dopaminergic innervation, notably in the FB [56]. The role of dopaminergic input in synaptic modulation and learning processes in the MB [57] suggests a similar role in the CX to generate a synaptic memory. This is consistent with observations that link the dopaminergic circuit in the CX to the regulation to wake/sleep arousal or stimulus specific arousal [58] and more generally its proposed function to modulate the arousal threshold in *Drosophila* [59].

3.2 An operant strategy to find where to go

The main principle of our model is the creation of the memory during the exploration of the surrounding environment under the influence of goodness/badness signals derived from innate and/or learned sensory preferences. The exploratory behaviour here is crucial, first supporting the scan of the surroundings and integrating the proprioception correctly (figure S.5) to ensure an optimal behaviour. Note that, although our model does not need any systematic scanning of the visual environment to decide the course to take [24], it is not able to provide a steering command to an orientation that has not been previously seen or scanned (some other proposed navigation models do have this capacity, e.g., by using the frequency transformation of the visual scenery [20; 60]). However, a large number of insect species express systematic scanning procedures before determining a route/direction to take [ants [61; 62]; dungbeetles [63], sandhoppers [64]], supporting our model assumptions. To create an exploratory behaviour in our simulation we add a fair amount of noise (gaussian noise with $s.d. = 10°$) to the steering behaviour, which appears to be crucial (figure S.6) to generate correct results. Adding a stochastic component as noise to the behaviour could be justified by locomotor mechanics or external disturbances. Alternatively, another option could be to use the oscillatory behaviour shown by wood ants [9]. This could provide a systematic and controlled exploration of their surroundings that would serve the same function. In addition, head movements and initial systematic scanning behaviour [61] could offer ways to increase the exploration of the environment while maintaining the course.

3.3 Why use the CX for innate attraction?

Our model focuses on the potential of the specific architecture of the CX to sustain different types of oriented behaviour (attraction, menotaxis, memory-guided relative to landmarks) based on sensory signals in the form of (undirected) attractiveness. As such, the EB is assumed to play a role even in the innate attraction to a visual landmark, which we assume induces a reward signal when appearing in a restricted area of the visual field ($\pm 15°$ of the frontal field of view), modulating the EP to PFL weights to cause steering towards it. In fact, in walking *Drosophila*, disrupting the EB function abolishes menotaxis but not direct attraction to a cue [16]. We believe it is highly likely that alternative direct sensory pathways for innate attraction exist simultaneously, able to control the behaviour without the need for an orientation representation provided by the CX [65]. The existence of direct connections from visual lobes to steering neurons downstream from the CX supports the existence of such pathway(s) [30]. However, a number of observations make it plausible to suppose that attraction to conspicuous cues could simultaneously involve memory related pathway(s) incorporating an orientation representation inherited from the CX [36], as this may offer several advantages.

One is the creation of a stable heading that can persist even with a disappearance of the cue(s) (figure S.7) as observed in *Drosophila* [46; 66], as long as the EB bump motion is supported by other cues (for example the proprioceptive cues maintaining heading tracking in darkness [13], figure 2D). Therefore, the CX could act as a smoothing filter, in addition to direct taxis mechanisms, to generate a short-term memory of the sensory world when this appears to be unsteady. Note that these advantages also apply to enhance either menotaxis or memory-guided orientation over a direct taxis system, e.g., smoothing the integration of the MB signals that can be unsteady [37]. The integration of a sparsely accessible sensory signals could be particularly interesting considering cluttered and unsteady environments where insects can forage. The ability of desert ants to perform homing while walking backwards would also benefit from a short term storage of the steering required for visual memory during punctual peeking phases [67].

The temporal integration at the CX level also makes possible to explore several innately attractive features of the environment and build-up a global direction vector combining them. This individual consideration of landmarks rather than the deciphering of the global layout of the environment would match some observation in insects [68; 69]. It is also noteworthy that attraction to vertical lines in wood ants has been proposed [70] to be sustained by their functional potential to resemble tree trunks (a key source of food) and therefore could be determined by early life experience. That is, the nature of the attractive target could become

refined as particular visual stimuli are discovered to be rewarding. This can be considered as a more general principle, in which a 'map' of the visual environment attractiveness [71] generates a heading vector, for any location, based on the EB bump. The same architecture could also be generalised to other sensory inputs [olfaction, wind sensing, ... (see figure S.8 for gradient ascent capability)] to generate such a combined heading vector (or a set of vectors) and enhance the robustness of the behaviour (see section 3.4).

3.4 Optimal sensory integration

In addition to its spatio-temporal properties, the integration of several sensory pathways on a single compass-driven scheme offers an interesting substrate to look further into optimization of the behaviour. Optimal integration in biological systems has been considered to conform to Bayesian principles [see [22; 72–74]; or a similar approach adapted to circular navigation [21]], as a principled way to take noise and uncertainty into account. Social insects and central-place foragers have evolved under high pressure to be able to return reliably to their nests, and hence make use of multiple redundant mechanisms, and a wide range of sensory cues including visual cues (polarised light, landmarks, sun, light gradients), magnetic fields, optic flow, odours, wind direction, tactile cues and/or proprioception [75; 76]. The problem of how these are combined for robust navigation has been considered in mathematical models [21] but how it might be realised in the brain of the animal is still unknown [20].

Here, the modulation over time of the weight distribution during the exploration of the sensory environment offers a way to generate directly a combined probablility distribution from multiple inputs. An example that we observe from our simulation is the impact of negative rewards in addition to positive ones to create the attraction to the landmark (figure 6). It has been recently shown in ants homing behaviour that memorizing anti-views or repellent memories to the nest (or to a goal), in addition to an attractive memory, could help them determining the course to take [2; 77]. The combination of these two opposed pathways on our synaptic memory model would automatically create a combined distribution (figure S.9) and improving the homing performance as proposed in [78].

Importantly, this use of two different reward signals could be directly extended to two (or more) rewards that come from different sensory systems. For example, if the agent was equipped with mechanosensors similar to insect antennae, we could define the equal deflection of both antennnae as rewarding, corresponding to an upwind heading direction. This could be combined with the existing reward when the visual landmark is centred, so that the two inputs simultaneously affect the adaptation of the weights. The relative strength of the two cues might then allow smooth transition between upwind flight when the visual stimulus is weak to visual attraction as this cue becomes stronger or more reliable.

Here we combined two different systems for visual reward, one innate and one learned. The interaction between innate and learned modalities is important for insect navigation [7; 76]. We considered the simplest case where the influence of each pathway is added linearly. The exploration of different integration strategies could help us better understand the interaction between innate and learned behaviours. We therefore believe that this model will help in exploring the ontogeny of the transformation from innate to learned landmark use [7; 79].

Aknowledgment

We are very thankful to Ioannis Pisokas for the discussions on the EB modeling and to James Knight for his comments on the manuscript. We acknowledge funding support from the Biotechnology and Biological Sciences Research Council [BB/R005036/1].

References

[1] Tessereau C, O'Dea R, Coombes S, Bast T. Reinforcement Learning approaches to hippocampus-dependent flexible spatial navigation. bioRxiv. 2020; p. 2020.07.30.229005. doi:10.1101/2020.07.30.229005.

[2] Wystrach A, Buehlmann C, Schwarz S, Cheng K, Graham P. Rapid aversive and memory trace learning during route navigation in desert ants. Current Biology. 2020;30(10):1927–1933.e2. doi:10.1016/j.cub.2020.02.082.

[3] Voss C. Über das Formensehen der roten Waldameise (Formica rufa-Gruppe). Zeitschrift für vergleichende Physiologie. 1967;55(3):225–254.

[4] Collett TS. Insect navigation en route to the goal: multiple strategies for the use of landmarks. Journal of Experimental Biology. 1996;199(1):227–235.

[5] Collett TS, Collett M. Memory use in insect visual navigation. Nature Reviews Neuroscience. 2002;3(7):542–552. doi:10.1038/nrn872.

[6] Graham P, Collett TS. View-based navigation in insects: how wood ants (*Formica rufa L.*) look at and are guided by extended landmarks. Journal of Experimental Biology. 2002;205(16):2499–2509.

[7] Graham P, Fauria K, Collett TS. The influence of beacon-aiming on the routes of wood ants. Journal of Experimental Biology. 2003;206(3):535–541. doi:10.1242/jeb.00115.

[8] Harris RA, Graham P, Collett TS. Visual cues for the retrieval of landmark memories by navigating wood ants. Current Biology. 2007;17(2):93–102. doi:10.1016/j.cub.2006.10.068.

[9] Collett TS, Lent DD, Graham P. Scene perception and the visual control of travel direction in navigating wood ants. Philosophical Transactions of the Royal Society B: Biological Sciences. 2014;369(1636):20130035. doi:10.1098/rstb.2013.0035.

[10] Bausenwein B, Müller NR, Heisenberg M. Behavior-dependent activity labeling in the central complex of *Drosophila* during controlled visual stimulation. Journal of Comparative Neurology. 1994;340(2):255–268. doi:https://doi.org/10.1002/cne.903400210.

[11] Buehlmann C, Wozniak B, Goulard R, Webb B, Graham P, Niven JE. Mushroom bodies are required for learned visual navigation, but not for innate visual behavior, in ants. Current Biology. 2020;30(17):3438–3443.e2. doi:10.1016/j.cub.2020.07.013.

[12] Jundi Be, Baird E, Byrne MJ, Dacke M. The brain behind straight-line orientation in dung beetles. Journal of Experimental Biology. 2019;222(Suppl 1). doi:10.1242/jeb.192450.

[13] Seelig JD, Jayaraman V. Neural dynamics for landmark orientation and angular path integration. Nature. 2015;521(7551):186–191. doi:10.1038/nature14446.

[14] Turner-Evans DB, Jayaraman V. The insect central complex. Current Biology. 2016;26(11):R453–R457.

[15] Tolman EC, Ritchie BF, Kalish D. Studies in spatial learning. I. Orientation and the short-cut. Journal of Experimental Psychology. 1946;36(1):13–24. doi:10.1037/h0053944.

[16] Green J, Vijayan V, Mussells Pires P, Adachi A, Maimon G. A neural heading estimate is compared with an internal goal to guide oriented navigation. Nature Neuroscience. 2019;22(9):1460–1468. doi:10.1038/s41593-019-0444-x.

[17] Giraldo YM, Leitch KJ, Ros IG, Warren TL, Weir PT, Dickinson MH. Sun navigation requires compass neurons in *Drosophila*. Current Biology. 2018;28(17):2845–2852.e4. doi:10.1016/j.cub.2018.07.002.

[18] Wolff T, Iyer NA, Rubin GM. Neuroarchitecture and neuroanatomy of the *Drosophila* central complex: A GAL4-based dissection of protocerebral bridge neurons and circuits. Journal of Comparative Neurology. 2015;523(7):997–1037. doi:https://doi.org/10.1002/cne.23705.

[19] Stone T, Webb B, Adden A, Weddig NB, Honkanen A, Templin R, et al. An anatomically constrained model for path integration in the bee brain. Current Biology. 2017;27(20):3069–3085.e11. doi:10.1016/j.cub.2017.08.052.

[20] Sun X, Yue S, Mangan M. A decentralised neural model explaining optimal integration of navigational strategies in insects. bioRxiv. 2020; p. 856153. doi:10.1101/856153.

[21] Hoinville T, Wehner R. Optimal multiguidance integration in insect navigation. Proceedings of the National Academy of Sciences. 2018;115(11):2824–2829. doi:10.1073/pnas.1721668115.

[22] Sun X, Mangan M, Yue S. An analysis of a ring attractor model for cue integration. In: Vouloutsi V, Halloy J, Mura A, Mangan M, Lepora N, Prescott TJ, et al., editors. Biomimetic and Biohybrid Systems. Lecture Notes in Computer Science. Cham: Springer International Publishing; 2018. p. 459–470.

[23] Peng F, Chittka L. A simple computational model of the bee mushroom body can explain seemingly complex forms of olfactory learning and memory. Current Biology. 2017;27(2):224–230. doi:10.1016/j.cub.2016.10.054.

[24] Ardin P, Peng F, Mangan M, Lagogiannis K, Webb B. Using an insect mushroom body circuit to encode route memory in complex natural environments. PLOS Computational Biology. 2016;12(2):e1004683. doi:10.1371/journal.pcbi.1004683.

[25] Pisokas I, Heinze S, Webb B. The head direction circuit of two insect species. eLife. 2020;9:e53985. doi:10.7554/eLife.53985.

[26] Hertz JA. Introduction to the theory of neural computation. CRC Press; 2018.

[27] Pfeiffer K, Homberg U. Organization and functional roles of the central complex in the insect brain. Annual Review of Entomology. 2014;59(1):165–184. doi:10.1146/annurev-ento-011613-162031.

[28] Kim SS, Rouault H, Druckmann S, Jayaraman V. Ring attractor dynamics in the *Drosophila* central brain. Science. 2017;356(6340):849–853. doi:10.1126/science.aal4835.

[29] Seelig JD, Jayaraman V. Feature detection and orientation tuning in the *Drosophila* central complex. Nature. 2013;503(7475):262–266. doi:10.1038/nature12601.

[30] Rayshubskiy A, Holtz SL, D'Alessandro I, Li AA, Vanderbeck QX, Haber IS, et al. Neural control of steering in walking *Drosophila*. bioRxiv. 2020; p. 2020.04.04.024703. doi:10.1101/2020.04.04.024703.

[31] Xu CS, Januszewski M, Lu Z, Takemura Sy, Hayworth KJ, Huang G, et al. A connectome of the adult *Drosophila* central brain. bioRxiv. 2020; p. 2020.01.21.911859. doi:10.1101/2020.01.21.911859.

[32] Milyaev N, Osumi-Sutherland D, Reeve S, Burton N, Baldock RA, Armstrong JD. The virtual fly brain browser and query interface. Bioinformatics. 2012;28(3):411–415. doi:10.1093/bioinformatics/btr677.

[33] Zheng Z, Lauritzen JS, Perlman E, Robinson CG, Nichols M, Milkie D, et al. A complete electron microscopy volume of the brain of adult *Drosophila melanogaster*. Cell. 2018;174(3):730–743.e22. doi:10.1016/j.cell.2018.06.019.

[34] Bogovic JA, Otsuna H, Heinrich L, Ito M, Jeter J, Meissner G, et al. An unbiased template of the Drosophila brain and ventral nerve cord. Plos one. 2020;15(12):e0236495.

[35] Buehlmann C, Woodgate J, Collett T. On the encoding of panorami visual scenes in navigating wood ants. Current Biology. 2016;26(15):2022–2027. doi:10.1016/j.cub.2016.06.005.

[36] Honkanen A, Adden A, Freitas JdS, Heinze S. The insect central complex and the neural basis of navigational strategies. Journal of Experimental Biology. 2019;222(Suppl 1). doi:10.1242/jeb.188854.

[37] Wystrach A, Moël FL, Clement L, Schwarz S. A lateralised design for the interaction of visual memories and heading representations in navigating ants. bioRxiv. 2020; p. 2020.08.13.249193. doi:10.1101/2020.08.13.249193.

[38] Endlein T, Sitti M. Innate turning preference of leaf-cutting ants in the absence of external orientation cues. Journal of Experimental Biology. 2018;221(14). doi:10.1242/jeb.177006.

[39] Kral K. Visually guided search behavior during walking in insects with different habitat utilization strategies. Journal of Insect Behavior. 2019;32(4):290–305. doi:10.1007/s10905-019-09735-8.

[40] Knaden M, Strutz A, Ahsan J, Sachse S, Hansson B. Spatial representation of odorant valence in an insect brain. Cell Reports. 2012;1(4):392–399. doi:10.1016/j.celrep.2012.03.002.

[41] Heisenberg M. Mushroom body memoir: from maps to models. Nature Reviews Neuroscience. 2003;4(4):266–275. doi:10.1038/nrn1074.

[42] Kamhi JF, Barron AB, Narendra A. Vertical lobes of the mushroom bodies are essential for view-based navigation in Australian *Myrmecia* ants. Current Biology. 2020;30(17):3432–3437.e3. doi:10.1016/j.cub.2020.06.030.

[43] Heinze S. Visual navigation: Ants lose track without mushroom bodies. Current Biology. 2020;30(17):R984–R986. doi:10.1016/j.cub.2020.07.038.

[44] Duistermars BJ, Chow DM, Frye MA. Flies require bilateral sensory input to track odor gradients in flight. Current Biology. 2009;19(15):1301–1307. doi:10.1016/j.cub.2009.06.022.

[45] Ofstad TA, Zuker CS, Reiser MB. Visual place learning in Drosophila melanogaster. Nature. 2011;474(7350):204–207.

[46] Neuser K, Triphan T, Mronz M, Poeck B, Strauss R. Analysis of a spatial orientation memory in Drosophila. Nature. 2008;453(7199):1244–1247.

[47] Dewar ADM, Wystrach A, Graham P, Philippides A. Navigation-specific neural coding in the visual system of Drosophila. Biosystems. 2015;136:120–127. doi:10.1016/j.biosystems.2015.07.008.

[48] Kim SS, Hermundstad AM, Romani S, Abbott LF, Jayaraman V. Generation of stable heading representations in diverse visual scenes. Nature. 2019;576(7785):126–131. doi:10.1038/s41586-019-1767-1.

[49] Maimon G, Straw AD, Dickinson MH. A simple vision-based algorithm for decision making in flying *Drosophila*. Current Biology. 2008;18(6):464–470.

[50] Borst A, Haag J. Neural networks in the cockpit of the fly. Journal of Comparative Physiology A. 2002;188(6):419–437.

[51] Young JM, Armstrong JD. Structure of the adult central complex in *Drosophila*: Organization of distinct neuronal subsets. Journal of Comparative Neurology. 2010;518(9):1500–1524. doi:https://doi.org/10.1002/cne.22284.

[52] Heinze S, Florman J, Asokaraj S, Jundi Be, Reppert SM. Anatomical basis of sun compass navigation II: The neuronal composition of the central complex of the monarch butterfly. Journal of Comparative Neurology. 2013;521(2):267–298. doi:https://doi.org/10.1002/cne.23214.

[53] Heinze S, Narendra A, Cheung A. Principles of insect path integration. Current Biology. 2018;28(17):R1043–R1058. doi:10.1016/j.cub.2018.04.058.

[54] Liu G, Seiler H, Wen A, Zars T, Ito K, Wolf R, et al. Distinct memory traces for two visual features in the *Drosophila* brain. Nature. 2006;439(7076):551–556. doi:10.1038/nature04381.

[55] Pan Y, Zhou Y, Guo C, Gong H, Gong Z, Liu L. Differential roles of the fan-shaped body and the ellipsoid body in Drosophila visual pattern memory. Learning & Memory. 2009;16(5):289–295. doi:10.1101/lm.1331809.

[56] Karam CS, Jones SK, Javitch JA. Come Fly with Me: An overview of dopamine receptors in Drosophila melanogaster. Basic & clinical pharmacology & toxicology. 2020;126:56–65.

[57] Berry JA, Cervantes-Sandoval I, Nicholas EP, Davis RL. Dopamine is required for learning and forgetting in Drosophila. Neuron. 2012;74(3):530–542.

[58] Lebestky T, Chang JSC, Dankert H, Zelnik L, Kim YC, Han KA, et al. Two different forms of arousal in Drosophila are oppositely regulated by the dopamine D1 receptor ortholog DopR via distinct neural circuits. Neuron. 2009;64(4):522–536.

[59] Van Swinderen B, Andretic R. Dopamine in Drosophila: setting arousal thresholds in a miniature brain. Proceedings of the Royal Society B: Biological Sciences. 2011;278(1707):906–913.

[60] Stone T, Mangan M, Wystrach A, Webb B. Rotation invariant visual processing for spatial memory in insects. Interface Focus. 2018;8(4):20180010. doi:10.1098/rsfs.2018.0010.

[61] Zeil J, Narendra A, Stürzl W. Looking and homing: how displaced ants decide where to go. Philosophical Transactions of the Royal Society B: Biological Sciences. 2014;369(1636):20130034. doi:10.1098/rstb.2013.0034.

[62] Wystrach A, Philippides A, Aurejac A, Cheng K, Graham P. Visual scanning behaviours and their role in the navigation of the Australian desert ant *Melophorus bagoti*. Journal of Comparative Physiology A. 2014;200(7):615–626. doi:10.1007/s00359-014-0900-8.

[63] Baird E, Byrne MJ, Smolka J, Warrant EJ, Dacke M. The dung beetle dance: An orientation behaviour? PLOS ONE. 2012;7(1):e30211. doi:10.1371/journal.pone.0030211.

[64] Ugolini A. Equatorial sandhoppers use body scans to detect the earth's magnetic field. Journal of Comparative Physiology A. 2006;192(1):45–49. doi:10.1007/s00359-005-0046-9.

[65] Gorostiza EA, Colomb J, Brembs B. A decision underlies phototaxis in an insect. Open Biology. 2016;6(12):160229. doi:10.1098/rsob.160229.

[66] Strauss R, Pichler J. Persistence of orientation toward a temporarily invisible landmark in Drosophila melanogaster. Journal of Comparative Physiology A. 1998;182(4):411–423.

[67] Schwarz S, Mangan M, Zeil J, Webb B, Wystrach A. How ants use vision when homing backward. Current Biology. 2017;27(3):401–407. doi:10.1016/j.cub.2016.12.019.

[68] Mizunami M, Weibrecht JM, Strausfeld NJ. Mushroom bodies of the cockroach: Their participation in place memory. Journal of Comparative Neurology. 1998;402(4):520–537. doi:https://doi.org/10.1002/(SICI)1096-9861(19981228)402:4¡520::AID-CNE6¿3.0.CO;2-K.

[69] Wessnitzer J, Mangan M, Webb B. Place memory in crickets. Proceedings of the Royal Society B: Biological Sciences. 2008;275(1637):915–921. doi:10.1098/rspb.2007.1647.

[70] Vowles DM. Maze learning and visual discrimination in the wood ant (*Formica rufa*). British Journal of Psychology. 1965;56(1):15–31. doi:https://doi.org/10.1111/j.2044-8295.1965.tb00940.x.

[71] Webb B. The internal maps of insects. Journal of Experimental Biology. 2019;222(Suppl 1). doi:10.1242/jeb.188094.

[72] Ernst MO, Bülthoff HH. Merging the senses into a robust percept. Trends in Cognitive Sciences. 2004;8(4):162–169. doi:10.1016/j.tics.2004.02.002.

[73] Arganda S, Pérez-Escudero A, Polavieja GGd. A common rule for decision making in animal collectives across species. Proceedings of the National Academy of Sciences. 2012;109(50):20508–20513. doi:10.1073/pnas.1210664109.

[74] Wystrach A, Mangan M, Webb B. Optimal cue integration in ants. Proceedings of the Royal Society B: Biological Sciences. 2015;282(1816):20151484. doi:10.1098/rspb.2015.1484.

[75] Heinze S. Unraveling the neural basis of insect navigation. Current Opinion in Insect Science. 2017;24:58–67. doi:10.1016/j.cois.2017.09.001.

[76] Buehlmann C, Mangan M, Graham P. Multimodal interactions in insect navigation. Animal Cognition. 2020;23(6):1129–1141. doi:10.1007/s10071-020-01383-2.

[77] Murray T, Kócsi Z, Dahmen H, Narendra A, Möel FL, Wystrach A, et al. The role of attractive and repellent scene memories in ant homing (*Myrmecia croslandi*). Journal of Experimental Biology. 2020;223(3). doi:10.1242/jeb.210021.

[78] Möel FL, Wystrach A. Opponent processes in visual memories: A model of attraction and repulsion in navigating insects' mushroom bodies. PLOS Computational Biology. 2020;16(2):e1007631. doi:10.1371/journal.pcbi.1007631.

[79] Collett M, Collett TS. How does the insect central complex use mushroom body output for steering? Current Biology. 2018;28(13):R733–R734. doi:10.1016/j.cub.2018.05.060.